LARGE DISPLACEMENT ELASTIC-PLASTIC ANALYSIS OF LAMINATED COMPOSITE PLATES UNDER IN-PLANE COMPRESSIVE LOADS

Dr. Husain M. Husain
Professor
in Civil Engineering,
University of Tekrit

Dr. Nameer A. Alwash
Professor
in Civil Engineering,
University of Babylon

Dr.Haider K. Ammash
Lecturer.
in Civil Engineering,
University of Al-Qadisiya

Abstract

A nonlinear finite element method is adopted for the large displacement elastic-plastic static analysis of anisotropic plates under in-plane compressive loads. The analysis is based on the two-dimensional layered approach with classical and higher order shear deformation theory with five, seven, and nine degrees of freedom per node. Nine-node Lagrangian isoparametric quadrilateral elements are used for the discretization of the laminated plates. Effects of orthotropy of individual layers, through-thickness shear deformation, fiber's orientation angle, and fiber waviness on the large displacement elastic-plastic static analysis are considered. The plate is analyzed with a range of number of sequences (***k***) of sine wave fiber (1-12) and with a range of the amplitude of fiber path (Δ) of sine wave fiber (0.0-0.5). The conclusion it is shown that the behavior of the laminated plate is very sensitive to the shape of fibers (straight or sine wave), also the behavior of the plate with sine wave fiber depends on the amplitude of the fiber and the number of sequences of the fiber, and so the capacity of the laminated plate with sine wave fiber and under in-plane compressive load in the direction of waviness is higher than the capacity of the plate with sine wave fiber and under in-plane compressive load orthogonal to the direction of waviness by approximate value (42%).

Keyword: Large Displacement, elastic-plastic analysis, finite element method, composite plate, in-plane compressive loads.

تحليل الإزاحة الكبيرة المرن-اللدن للصفائح غير متماثلة الخواص تحت تأثير حمل ضغط في المستوي

د. حسين محمد حسين
أستاذ/جامعة تكريت

د. نمير عبد الأمير علوش
أستاذ مساعد/جامعة بابل

د.حيدر كاظم عماش
مدرس/جامعة القادسية

الخلاصة:-

تم تقديم طريقة العناصر المحددة اللاخطية لتحليل الإزاحة الكبيرة المرن-اللدن الاستاتيكي للصفائح غير متماثلة الخواص تحت حمل ضغط في المستوي. تبنت هذه الدراسة طريقة الطبقة ثنائي البعد(two-dimensional layered approach) واعتمدت نظرية التشوهات القصية الكلاسيكية وذات المرتبة العليا (classical and higher order shear deformation theory) مع خمس،وسبع وتسع درجات حرية لكل عقدة، تم توظيف عنصر لاكرانج (Lagrangian) ذي العقد التسع لتمثيل الصفائح الطبقية. وقد أُخذ بنظر الاعتبار تأثيرتعامد الخواص للطبقات المنفردة وزاوية تدوير الألياف وتموج الألياف على تحليل الإزاحة الكبيره المرن-اللدن الاستاتيكي. تم تحليل الصفيحة مع مجال من تسلسل الالياف المتموجة (1-12)، ومجال من ارتفاع قمة الالياف

المتموجة(0.0-0.5). من النتائج المستحصلة، يمكن ملاحظة ان تصرف الصفائح الطبقية حساس جداً لشكل الالياف (مستقيم او متموج). وأيضا تصرّف الصفائح ذات الالياف المتموجة معتمد على ارتفاع قمة الالياف وعدد تسلسل التموجات'وكذلك ان قابلية التحمل للصفائح المُطبّقة والمتموجة الالياف وتحت حمل ضغط في اتجاه التموج اكثر من قابلية التحمل للصفائح الطبقية والمتموجة الالياف وتحت حمل ضغط عمودي على التموج بحوالي (42%).

Notations

Symbol	Description
a, b	Plate dimensions in *x* and *y*-directions, respectively.
$[B]$	Strain-nodal displacement matrix.
D	Flexural rigidity = $Et^3/12(1-\nu^2)$.
E_i	Modulus of elasticity in i-direction.
E_f	Modulus of elasticity of fiber.
E_m	Modulus of elasticity of matrix.
F_i, F_{ij}	Strength tensors of the first and second order, respectively.
$\{F\}$	External load vector.
F	Yield function.
G	Shear modulus.
h_L-h_{L-1}	Distance from plate middle surface to the upper and lower surface of L^{th} lamina.
h	Plate thickness.
$[K_o]$	Constant linear elastic stiffness matrix
$[K_L]$	Initial or large displacement matrix
$[K_\sigma]$	Initial stress stiffness matrix
$[K_T]_0$	Tangent stiffness matrix.
M_x, M_y, M_{xy}	Bending and twisting moments (per unit width) (on *yz*, *xz*, and both *yz* and *xz*-sections).
M_x^*, M_y^*, M_{xy}^*	Higher order bending and twisting moments (per unit width) (on *yz*, *xz*, and both *yz* and *xz*-sections).
N_x, N_y, N_{xy}	In-plane stress resultants (per unit width) (on *yz*, *xz*, and both *yz* and *xz*-sections).
N_x^*, N_y^*, N_{xy}^*	Higher order in-plane stress resultants (per unit width) (on *yz*, *xz*, and both *yz* and *xz*-sections).
P_x	In-plane applied load in *x*-direction.
Q_x, Q_y	Transverse shearing forces (per unit width) (on *yz* and *xz*-sections).
w_o	Amplitude of initial imperfection.
x,y,z	Coordinates.
γ_{ij}^o	Shear strain in ij-plane at middle surface.
γ_{ij}^{o*}	Higher order shear strain in ij-plane at middle surface.
$\{\varepsilon\}$	Strain vector.
$\{\varepsilon_o\}$	Middle surface strain vector.
ε_i	Normal strain in i-direction.
ε_i^o	Normal strain in i-direction at middle surface.
ε_i^{o*}	Higher order normal strain in i-direction at middle surface.

ξ,η	Curvilinear coordinates system.
θ	Fiber's orientation angle.
θ_x,θ_y	Rotations of transverse normals in the (*xz*) and (*yz*) planes.
θ_x^*,θ_y^*	Higher order rotations of transverse normals in the (*xz*) and (*yz*) planes.
κ_i^o	Bending curvature in i-plane at middle surface.
κ_{ij}^o	Bending curvature in ij-plane at middle surface.
κ_i^{o*}	Higher order bending curvature in i-plane at middle surface.
κ_{ij}^{o*}	Higher order bending curvature in ij-plane at middle surface.
ν_i	Poisson's ratio in i-direction.
σ_o	Yield stress of steel

Introduction

The composite material is made of two or more macro-constituent's materials essentially soluble or mixable into each other, usually a reinforcing material supported in a compatible matrix, where the sum of properties of each constituent taken separately, are assembled in prescribed amounts to achieve specific physical and chemical properties [**Jones,1999**][9].

The reinforcement materials may form as continuous or discontinuous fibers, flakes, fillers or particles embedded in the matrix material. Fibers in various forms (mat yarn, woven roving, and chopped strands) are inherently much stiffer and stronger than the same material in bulk form. The matrix material works as a binder material giving the composite a protection and supports its bulk form and stress transfer when the fiber is broken. Typically, the matrix is of considerably lower density, stiffness and strength than those of the fibers.

Layered composite material plates are extensively used in the construction of aerospace, civil, marine, automotive and other high performance structures, and during the operation of this structure, it is subjected to static and dynamic loads, as shown in **Figure (1)**. Therefore, there exists a need for investigating the response of layered (laminated) composite material plates subjected to such types of loading.

The finite element method has been applied with great success to geometrical and material nonlinearities in continuum and structural problems. The geometric nonlinearity is modeled by well-known formulations, the total or updated Lagrangian coordinates, while success in modeling the material nonlinearities depends on the validity of the constitutive models to be used. **Elseifi** [**1998**][7] presented nonlinear finite element method for the post-buckling analysis of stiffened composite panels with geometric imperfections. A four node, six degrees of freedom per node, rectangular, conformal element was used. Transverse shear effects were neglected since the width to thickness ratio of the panels under consideration is over 500. A maximum stress failure criterion was added to the finite element code to predict the panel post-buckling failure load. A new integration technique that mixes symbolic closed-form function manipulation and Gaussian quadrature numerical integration had been introduced in order to reduce the required computation time for each analysis. His study did not take the effect of fiber orientation, number of fibers, and type of initial imperfection. **Shukla** and **Nath** [**2000**][15] presented a post-buckling analysis of shear deformable cross-ply laminated rectangular plate subjected to the combination of in-plane edge compressive mechanical loading and thermal loads due to a linearly varying temperature across the thickness. Their formulation was based on the first order shear deformation theory and Von-Karman type nonlinearity. They observed that their present method was quite efficient in obtaining the buckling and post-buckling response of a laminated composite plate under thermomechanical

loading. More recently, **Zou** and **Qiao** [**2002**][16] presented a higher order finite strip method for post-buckling behavior of imperfect composite plates subjected to progressive end shortening. The arbitrary nature of initial geometric imperfection induced during manufacturing was accounted for in the analysis. The nonlinear equilibrium equations were solved by Newton-Raphson method. That study showed that the post-buckling behavior of an imperfect composite plate depends not only on the material lay up, snap-to-thickness and anisotropy of the laminate, but also on the direction of induced out-of-plane imperfection. From the preceding review of literature, it is clear that there is no study which considers the nonlinear static analysis of isolated laminated plate under axial compression load by taking into account the effect of type of fiber (straight or wavy). There is also a little amount of literature that takes into account the higher order displacement model of nine degrees of freedom per node with different types of lamination.

Laminated Plate Theories

A laminated plate is a series of laminas bonded together to act as an integral structural element. Thus, a laminate is not a material but instead a structural element with essential features of both material properties and geometry. The stiffness and strength of such a composite material with structural configuration are obtained from the properties of the constituent laminas, and thus the macromechanical behavior of a laminate is the main topic of this section. The lamination so described can be considered as a single layer with "rule of mixtures" representation of the interaction between the multiple laminas in a plate or shell [**Jones, 1999**][9].

There are two categories of theories, equivalent single layer and three dimensional elasticity theories. In the first category, the material properties of the constituent layer are smeared to form a hypothetical single layer whose properties are equivalent to through thickness integrated sum of its constituents, and this category contains classical lamination theory, first order shear deformation theory, and higher order shear deformation theory. The higher order shear deformation theories are more efficient to represent the transverse shear deformation, through-thickness displacement and strains. The assumption of a higher order plate theory can also be used within the equivalent layer formulation [**Jones, 1999**][9]. The strain expressions derived from the displacement field were considered by **[Ali, 2004**][2] with nine degrees of freedom per node as follows:

$$\begin{aligned} u(x,y,z,t) &= u_o(x,y,t) + z\theta_x(x,y,t) + z^2 u_o^*(x,y,t) + z^3\theta_x^*(x,y,t) \\ v(x,y,z,t) &= v_o(x,y,t) + z\theta_y(x,y,t) + z^2 v_o^*(x,y,t) + z^3\theta_y^*(x,y,t) \\ w(x,y,z,t) &= w_o(x,y,t) \end{aligned} \qquad (1)$$

in which the parameters (u, v, w, θ_x, θ_y, θ_x^*, and θ_y^*) are defined previously, u_o^*, and v_o^* are the corresponding higher order terms in Taylor's series expression and they are also defined at the middle plane. The strain-displacement relations after differentiating Equation (1) are:

$$\begin{aligned} \varepsilon_x &= \frac{\partial u}{\partial x} = \varepsilon_x^o + z\kappa_x + z^2\varepsilon_x^{o^*} + z^3\kappa_x^* \\ \varepsilon_y &= \frac{\partial v}{\partial y} = \varepsilon_y^o + z\kappa_y + z^2\varepsilon_y^{o^*} + z^3\kappa_y^* \\ \gamma_{xy} &= \frac{\partial u}{\partial y} + \frac{\partial v}{\partial x} = \gamma_{xy}^o + z\kappa_{xy} + z^2\gamma_{xy}^{o^*} + z^3\kappa_{xy}^* \\ \gamma_{xz} &= \frac{\partial u}{\partial z} + \frac{\partial w}{\partial x} = \varphi_x + z\gamma_{xz}^o + z^2\varphi_x^* \\ \gamma_{yz} &= \frac{\partial v}{\partial z} + \frac{\partial w}{\partial y} = \varphi_y + z\gamma_{yz}^o + z^2\varphi_y^* \end{aligned} \qquad (2)$$

Where

$$\varepsilon_x^o = \frac{\partial u_o}{\partial x},\ \varepsilon_y^o = \frac{\partial v_o}{\partial y},\ \gamma_{xy}^o = \frac{\partial u_o}{\partial y} + \frac{\partial v_o}{\partial x}$$

$$\kappa_x = \frac{\partial \theta_x}{\partial x},\ \kappa_y = \frac{\partial \theta_y}{\partial y},\ \kappa_{xy} = \frac{\partial \theta_x}{\partial y} + \frac{\partial \theta_y}{\partial x}$$

$$\varphi_x = \theta_x + \frac{\partial w_o}{\partial x}$$

$$\varphi_y = \theta_y + \frac{\partial w_o}{\partial y} \qquad (3)$$

$$\varepsilon_x^{o*} = \frac{\partial u_o^*}{\partial x},\ \varepsilon_y^{o*} = \frac{\partial v_o^*}{\partial y},\ \gamma_{xy}^{o*} = \frac{\partial u_o^*}{\partial y} + \frac{\partial v_o^*}{\partial x}$$

$$\gamma_{xz}^{o*} = 2u_o^*$$

$$\gamma_{yz}^{o*} = 2v_o^*$$

Also, all the strains above are defined in the middle-plane of the laminate. By substitution from Equation (3) into the stress-strain relations given by the following Equation:

$$\begin{bmatrix} \sigma_x \\ \sigma_y \\ \tau_{xy} \\ \tau_{xz} \\ \tau_{yz} \end{bmatrix} = \begin{bmatrix} Q_{11} & Q_{12} & Q_{16} & 0 & 0 \\ Q_{12} & Q_{22} & Q_{26} & 0 & 0 \\ Q_{16} & Q_{26} & Q_{66} & 0 & 0 \\ 0 & 0 & 0 & Q_{55} & Q_{45} \\ 0 & 0 & 0 & Q_{45} & Q_{44} \end{bmatrix} \begin{bmatrix} \varepsilon_x \\ \varepsilon_y \\ \gamma_{xy} \\ \gamma_{xz} \\ \gamma_{yz} \end{bmatrix} \qquad (4)$$

After complete integration, the stress-resultant/strain relations of the laminate are as follows[4]:

$$\begin{bmatrix} N_x \\ N_y \\ N_{xy} \\ N_x^* \\ N_y^* \\ N_{xy}^* \\ M_x \\ M_y \\ M_{xy} \\ M_x^* \\ M_y^* \\ M_{xy}^* \end{bmatrix} = \begin{bmatrix} A_{11} & A_{12} & A_{16} & D_{11} & D_{12} & D_{16} & B_{11} & B_{12} & B_{16} & E_{11} & E_{12} & E_{16} \\ A_{12} & A_{22} & A_{26} & D_{12} & D_{22} & D_{26} & B_{12} & B_{22} & B_{26} & E_{12} & E_{22} & E_{26} \\ A_{16} & A_{26} & A_{66} & D_{16} & D_{26} & D_{66} & B_{16} & B_{26} & B_{66} & E_{16} & E_{26} & E_{66} \\ D_{11} & D_{12} & D_{16} & F_{11} & F_{12} & F_{16} & E_{11} & E_{12} & E_{16} & G_{11} & G_{12} & G_{16} \\ D_{12} & D_{22} & D_{26} & F_{12} & F_{22} & F_{26} & E_{12} & E_{22} & E_{26} & G_{12} & G_{22} & G_{26} \\ D_{16} & D_{26} & D_{66} & F_{16} & F_{26} & F_{66} & E_{16} & E_{26} & E_{66} & G_{16} & G_{26} & G_{66} \\ B_{12} & B_{12} & B_{16} & E_{11} & E_{12} & E_{16} & D_{11} & D_{12} & D_{16} & F_{11} & F_{12} & F_{16} \\ B_{12} & B_{22} & B_{26} & E_{12} & E_{22} & E_{26} & D_{12} & D_{22} & D_{26} & F_{12} & F_{22} & F_{26} \\ B_{16} & B_{26} & B_{66} & E_{16} & E_{26} & E_{66} & D_{16} & D_{26} & D_{66} & F_{16} & F_{26} & F_{66} \\ E_{11} & E_{12} & E_{16} & G_{11} & G_{12} & G_{16} & F_{11} & F_{12} & F_{16} & H_{11} & H_{12} & H_{16} \\ E_{12} & E_{22} & E_{26} & G_{12} & G_{22} & G_{26} & F_{12} & F_{22} & F_{26} & H_{12} & H_{22} & H_{26} \\ E_{16} & E_{26} & E_{66} & G_{16} & G_{26} & G_{66} & F_{16} & F_{26} & F_{66} & H_{16} & H_{26} & H_{66} \end{bmatrix} \begin{bmatrix} \varepsilon_x^o \\ \varepsilon_y^o \\ \gamma_{xy}^o \\ \varepsilon_x^{o*} \\ \varepsilon_y^{o*} \\ \gamma_{xy}^{o*} \\ \kappa_x \\ \kappa_y \\ \kappa_{xy} \\ \kappa_x^* \\ \kappa_y^* \\ \kappa_{xy}^* \end{bmatrix} \qquad (5)$$

and,

$$\begin{bmatrix} Q_x \\ Q_y \\ S_x \\ S_y \\ Q_x^* \\ Q_y^* \end{bmatrix} = \begin{bmatrix} A_{55} & A_{45} & B_{55} & B_{45} & D_{55} & D_{45} \\ A_{45} & A_{44} & B_{45} & B_{44} & D_{45} & D_{44} \\ B_{55} & B_{45} & D_{55} & D_{45} & E_{55} & E_{45} \\ B_{45} & B_{44} & D_{45} & D_{44} & E_{45} & E_{44} \\ D_{55} & D_{45} & E_{55} & E_{45} & F_{55} & F_{45} \\ D_{45} & D_{44} & E_{45} & E_{44} & F_{45} & F_{44} \end{bmatrix} \begin{bmatrix} \varphi_x \\ \varphi_y \\ \gamma_{xz}^{o*} \\ \gamma_{yz}^{o*} \\ \varphi_x^* \\ \varphi_y^* \end{bmatrix} \qquad (6)$$

all coefficients in ***A***, ***B***, ***D***, ***E***, ***F***, ***G***, and ***H*** groups are defined as follows:

$$A_{ij} = \sum_{L=1}^{NL} Q_{ij}(h_L - h_{L-1}) \qquad i, j = 1, 2, 6 \text{ or } i, j = 4, 5 \qquad \textbf{(7 a)}$$

$$B_{ij} = (1/2)\sum_{L=1}^{NL} Q_{ij}(h_L^2 - h_{L-1}^2) \qquad i, j = 1, 2, 6 \text{ or } i, j = 4, 5 \qquad \textbf{(7 b)}$$

$$D_{ij} = (1/3)\sum_{L=1}^{NL} Q_{ij}(h_L^3 - h_{L-1}^3) \qquad i, j = 1, 2, 6 \text{ or } i, j = 4, 5 \qquad \textbf{(7 c)}$$

$$E_{ij} = (1/4)\sum_{L=1}^{NL} Q_{ij}(h_L^4 - h_{L-1}^4) \qquad i, j = 1, 2, 6 \text{ or } i, j = 4, 5 \qquad \textbf{(7 d)}$$

$$F_{ij} = (1/5)\sum_{L=1}^{NL} Q_{ij}(h_L^5 - h_{L-1}^5) \qquad i, j = 1, 2, 6 \text{ or } i, j = 4, 5 \qquad \textbf{(7 e)}$$

$$G_{ij} = (1/6)\sum_{L=1}^{NL} Q_{ij}(h_L^6 - h_{L-1}^6) \qquad i, j = 1, 2, 6 \qquad \textbf{(7 f)}$$

$$H_{ij} = (1/7)\sum_{L=1}^{NL} Q_{ij}(h_L^7 - h_{L-1}^7) \qquad i, j = 1, 2, 6 \qquad \textbf{(7 g)}$$

The present study explores the idea of tailoring the profile of reinforcing fibers to improve the buckling strength of composite plates. This study investigates the effect of waviness of fibers on the post buckling curves, as shown in Figure (4), and this waviness is of the form:

$$y(x) = \alpha \sin\left(\frac{k\pi x}{a}\right) \qquad \textbf{(8)}$$

such that the angle of fiber orientation θ varies along the longitudinal x-axis as:

$$\tan(\theta) = \frac{dy}{dx} = \frac{\alpha k\pi}{a}.\cos\left(\frac{k\pi x}{a}\right) = \Delta k\pi.\cos(k\pi\bar{x}) \qquad \textbf{(9)}$$

where a = plate length; k= number of half sine waves; and α= wave amplitude. Two normalized variables, $\Delta=\alpha/a$ and $\bar{x} = x/a$, are introduced.

The main objective is to study the effect of fiber waviness, characterized by k and Δ, on the static and dynamic buckling behavior of composite laminates. The fiber can also be rotated in any direction with the x-axis, as shown in Figure (4), by using the following expression:

$$x_n = x\cos(\beta) + y\sin(\beta) \qquad \textbf{(10)}$$

where x_n represent the x-coordinate for a rotated fiber, and β is the angle of the waviness fiber.

The angle of fiber orientation in Equation (9) is variable with x-coordinate and instead of the constant angle used for straight fibers.

Figure (5) shows the principal material directions aligned with the lamina axes by angle (β).

Geometrical Nonlinearity

The components of the Green-Lagrangian strain vector are known in terms of local derivatives of the displacements for the plate element as [**Pica**, **et al.**, **1979**][13]:

$$[\varepsilon] = \begin{Bmatrix} \varepsilon_x \\ \varepsilon_y \\ \gamma_{xy} \\ \gamma_{xz} \\ \gamma_{yz} \end{Bmatrix} = \begin{Bmatrix} \varepsilon_o^p \\ 0 \end{Bmatrix} + \begin{Bmatrix} z\varepsilon_o^b \\ \varepsilon_o^s \end{Bmatrix} + \begin{Bmatrix} \varepsilon_L^P \\ 0 \end{Bmatrix} + \begin{Bmatrix} \varepsilon_I^p \\ 0 \end{Bmatrix} \qquad \textbf{(11)}$$

where the linear mid-plane strains are:

$$\left[\varepsilon_o^p\right]=\begin{Bmatrix}\dfrac{\partial u}{\partial x}\\ \dfrac{\partial v}{\partial y}\\ \dfrac{\partial u}{\partial y}+\dfrac{\partial v}{\partial x}\end{Bmatrix} \quad (12)$$

Equation (12) represents the in-plane strain. Also:

$$\left[\varepsilon_o^b\right]=\begin{Bmatrix}\dfrac{\partial \theta_x}{\partial x}\\ \dfrac{\partial \theta_y}{\partial y}\\ \dfrac{\partial \theta_x}{\partial y}+\dfrac{\partial \theta_y}{\partial x}\end{Bmatrix} \quad (13)$$

Equation (13) represents the bending strain. Also:

$$\left[\varepsilon_o^s\right]=\begin{Bmatrix}\varphi_x\\ \varphi y\end{Bmatrix} \quad (14)$$

Equation (14) represents the shear strain. Moreover:

$$\left[\varepsilon_L^p\right]=\begin{Bmatrix}\dfrac{1}{2}\left(\dfrac{\partial w}{\partial x}\right)^2\\ \dfrac{1}{2}\left(\dfrac{\partial w}{\partial y}\right)^2\\ \dfrac{\partial w}{\partial x}\dfrac{\partial w}{\partial y}\end{Bmatrix} \quad (15)$$

Equation (15) represents the nonlinear component of in-plane strain. Finally:

$$\left[\varepsilon_I^p\right]=\begin{Bmatrix}\dfrac{\partial w}{\partial x}\dfrac{\partial w_o}{\partial x}\\ \dfrac{\partial w}{\partial y}\dfrac{\partial w_o}{\partial y}\\ \dfrac{\partial w}{\partial x}\dfrac{\partial w_o}{\partial y}+\dfrac{\partial w_o}{\partial x}\dfrac{\partial w}{\partial y}\end{Bmatrix} \quad (16)$$

Equation (16) represents the initial strain due to initial deflection. The vector components of Equation (11) represent the generalized strains. It can be noted that the vector $(\varepsilon_p^o+\varepsilon_L^p+\varepsilon_L^p)$ reproduce the Marguerre strain expression for plate.

Variational Equation of Equilibrium

The variation of strain $d\varepsilon$ due to the virtual displacements du, generally $d\varepsilon$ is given as the sum of the variation of the linear and nonlinear generalized strains as:

$$d\bar{\varepsilon}=d\varepsilon_o+d\varepsilon_L \quad (17)$$

Since ε_o is a linear function of displacement,

$$d\varepsilon_o=[B_o]du \quad (18)$$

Also,

$$d\varepsilon_L=[B_L]du \quad (19)$$

Thus, the total strain-nodal displacement matrix for total strains is:

$$[\overline{B}] = [B_o] + [B_L] \quad (20)$$

in which $[B_o]$ is the same matrix as in the linear strain analysis and $[B_L]$ depends on the displacements.

$$[B_o] = \begin{bmatrix} B_o^p & 0 \\ 0 & B_o^b \end{bmatrix}, \quad [B_L] = \begin{bmatrix} 0 & B_L^b \\ 0 & 0 \end{bmatrix} \quad (21)$$

where $[B_L]$ can be found by taking the variation of the nonlinear strain components $\{\varepsilon_L^p\}$ with respect to the displacements. This nonlinear strain components of Equation (11) can be written in a more convenient form as:

$$[\varepsilon_L^p] = \begin{Bmatrix} \frac{1}{2}\left(\frac{\partial w}{\partial x}\right)^2 \\ \frac{1}{2}\left(\frac{\partial w}{\partial y}\right)^2 \\ \left(\frac{\partial w}{\partial x}\right)\left(\frac{\partial w}{\partial y}\right) \end{Bmatrix} = \frac{1}{2}\begin{bmatrix} \frac{\partial w}{\partial x} & 0 \\ 0 & \frac{\partial w}{\partial y} \\ \frac{\partial w}{\partial y} & \frac{\partial w}{\partial x} \end{bmatrix} \begin{Bmatrix} \frac{\partial w}{\partial x} \\ \frac{\partial w}{\partial y} \end{Bmatrix} = \frac{1}{2}[A_\theta]\{\theta\} \quad (22)$$

where the displacement gradients with respect to the lateral displacements (w) are:

$$\{\theta\} = \begin{bmatrix} \frac{\partial w}{\partial x} \\ \frac{\partial w}{\partial y} \end{bmatrix} \quad (23)$$

Then, the variation of the nonlinear component of the in-plane strain is obtained from Equation (22) in terms of the virtual gradients $d\theta$ as:

$$d\varepsilon_L^p = A_\theta \, d\theta \quad (24)$$

where

$$A_\theta = \begin{bmatrix} \frac{\partial w}{\partial x} & 0 \\ 0 & \frac{\partial w}{\partial y} \\ \frac{\partial w}{\partial y} & \frac{\partial w}{\partial x} \end{bmatrix} \quad (25)$$

in which, A_θ represents the gradients of total displacements and,

$$d\theta = d\begin{bmatrix} \frac{\partial w}{\partial x} \\ \frac{\partial w}{\partial y} \end{bmatrix} \quad (26)$$

represents the gradients of incremental displacements.

The displacement gradients (θ) of Equation (23) may now be written in terms of the nodal displacements (u) and Cartesian derivatives of the shape functions as:

$$\{\theta\} = [G]\{u\} \quad (27)$$

where

$$[G] = [G_1 \quad G_2 \quad ..... \quad G_n] \quad (28)$$

and,

$$G_i = \begin{bmatrix} 0 & 0 & \dfrac{\partial N_i}{\partial x} & 0 & 0 \\ 0 & 0 & \dfrac{\partial N_i}{\partial y} & 0 & 0 \end{bmatrix} \quad (29)$$

The above equation represents the gradient for five degrees of freedom per node. Taking the variation of Equation (22) as follows:

$$d\{\varepsilon_L^p\} = \frac{1}{2} d[A_\theta]\{\theta\} + \frac{1}{2}[A_\theta] d\{\theta\} = [A_\theta] d\{\theta\} = [A_\theta][G] d\{u\} \quad (30)$$

hence immediately, by definition

$$[B_L^b]_o = [A_\theta][G] \quad (31)$$

In order to incorporate the imperfections in the formulation, the strain due to imperfections as given in Equation (11), thus can be written the imperfection strain components as follows:

$$\{\varepsilon_p^I\} = \frac{1}{2} \begin{bmatrix} 2\dfrac{\partial w_o}{\partial x} & 0 \\ 0 & 2\dfrac{\partial w_o}{\partial y} \\ 2\dfrac{\partial w_o}{\partial y} & 2\dfrac{\partial w_o}{\partial x} \end{bmatrix} \begin{Bmatrix} \dfrac{\partial w}{\partial x} \\ \dfrac{\partial w}{\partial y} \end{Bmatrix} = \frac{1}{2}[A_1]\{\theta\} \quad (32)$$

Following the same analysis as for the nonlinear strains, the combination of the effects of the two strains into one $[B_L^b]$ is defined as:

$$[B_L^b] = [A_2][G] \quad (33)$$

where

$$[A_2] = [A_\theta] + [A_1]$$

$$[A_2] = \begin{bmatrix} \dfrac{\partial w}{\partial x} + 2\dfrac{\partial w_o}{\partial x} & 0 \\ 0 & \dfrac{\partial w}{\partial y} + 2\dfrac{\partial w_o}{\partial y} \\ \dfrac{\partial w}{\partial y} + 2\dfrac{\partial w_o}{\partial y} & \dfrac{\partial w}{\partial x} + 2\dfrac{\partial w_o}{\partial x} \end{bmatrix} \quad (34)$$

In the present study, the imperfection is assumed to be of sinusoidal function over the plate as:

$$w_o(x,y) = w_o \sin\left(\frac{n\pi x}{L_x}\right) \sin\left(\frac{n\pi y}{L_y}\right) \quad (35)$$

where L_x, and L_y are the dimensions of the plate in the x, and y-direction, respectively. w_o is the maximum value of the initial imperfection at the plate center.

The variation in the potential energy of deformation for a plate element with large deflection can be written as:

$$dU = \int_V [\bar{B}]^T \sigma \, dV \quad (36)$$

Substituting Equations (36) can give the equilibrium equations written as:

$$\Psi(u) = \int_V [\bar{B}]^T \bar{\sigma} \, dV - dW = 0 \quad (37)$$

where Ψ represents the sum of external and internal generalized forces.

Clearly, the solution of Equation (37) will have to be approached iteratively. In order to use an incremental solution procedure, the relation between du and $d\Psi$ must be found. Thus, taking appropriate variation of Equation (37) with respect to du:

$$\frac{d\Psi}{du} = \int_V \frac{d[\bar{B}]^T}{du} \bar{\sigma}\, dV + \int_V [\bar{B}]^T \frac{d\bar{\sigma}}{du} dV \qquad (38)$$

where the variation of the external load with respect to displacements is equal to zero, and thus Equation (38) can be written at another form:

$$\frac{d\Psi}{du} = \int_V \frac{d[B_L]^T}{du} \bar{\sigma}\, dV + [\bar{K}] \qquad (39)$$

where

$$[\bar{K}] = \int_A [\bar{B}]^T [D][\bar{B}] dA = [K_o] + [K_L] \qquad (40)$$

The first term of Equation (39) can be written as:

$$\int_V \frac{d[B_L]^T}{du} \bar{\sigma}\, dV = [K_\sigma] \qquad (41)$$

where $[K_\sigma]$ is a symmetric matrix dependent on the stress level. This matrix is known as initial stress matrix or geometric matrix. Thus,

$$d\Psi = ([K_o] + [K_L] + [K_\sigma])\, du = [K_T]\, du \qquad (42)$$

with $[K_T]$ being the total, or tangent stiffness matrix.

Tangent Stiffness Matrix

The tangent stiffness matrix can be written as:

$$[K_T] = [K_o] + [K_L] + [K_\sigma] \qquad (43)$$

where $[K_o]$ is the constant linear elastic stiffness matrix and can be written as:

$$[K_o] = \int_A [B_o]^T [D][B_o] dA \qquad (44)$$

$[K_L]$ is the initial or large displacement matrix which is quadratically dependent upon displacement u, and can be written as:

$$[K_L] = \int_A [B_o]^T [D][B_L] dA + \int_A [B_L]^T [D][B_L] dA + \int_A [B_L]^T [D][B_o] dA \qquad (45)$$

Finally $[K_\sigma]$ is the initial stress stiffness matrix which has to be found by using the definition of Equation (41). By taking the variation of Equation (20) then:

$$d[B_L]^T = \begin{bmatrix} 0 & 0 \\ d[B_L^b]^T & 0 \end{bmatrix} \qquad (46)$$

This on substitution into Equations (41) and (34) gives:

$$[K_\sigma] = \int_A \begin{bmatrix} 0 & 0 \\ [G]^T d[A]^T & 0 \end{bmatrix} \begin{Bmatrix} N_x \\ N_y \\ N_{xy} \\ M_x \\ M_y \\ M_{xy} \end{Bmatrix} \qquad (47)$$

However, using the mathematical properties of the matrix **[*A*]**, this matrix can be written as:

$$d[A]^T \begin{Bmatrix} N_x \\ N_y \\ N_{xy} \end{Bmatrix} = \begin{bmatrix} N_x & N_{xy} \\ N_{xy} & N_y \end{bmatrix} [G] da \qquad \textbf{(48)}$$

and finally one can obtain

$$[K_\sigma] = \begin{bmatrix} 0 & 0 \\ 0 & [K_\sigma^b] \end{bmatrix} \qquad \textbf{(49)}$$

Thus,

$$[K_\sigma] = \int_A [G]^T \begin{bmatrix} N_x & N_{xy} \\ N_{xy} & N_y \end{bmatrix} [G] da \qquad \textbf{(50)}$$

Failure criteria for laminated plate structure

The stresses in an individual lamina are fundamental to control the failure initiation and progression in the laminate. The strength of each individual lamina is assessed separately by considering the stresses acting on it along the material axes. The initial failure of a lamina is governed by exceeding the maximum limit prescribed by a failure criterion. The determination of failure load is very essential in understanding the failure process as well as the reliability and safety of structures. The ultimate load that makes the plate fail is calculated based on **Tsai-Wu** criterion for general composite materials and on **Hashin** criterion for fiber composite materials as follows [**Jones**, **1999**][9]:

$$F_i \sigma_i + F_{ij} \sigma_i \sigma_j = 1; \qquad i, j = 1,.....,6 \qquad \textbf{(51)}$$

where F_i and F_{ij} are strength tensors of the second and fourth order respectively and the usual contracted tensor notation is used except that $\sigma_4 = \tau_{13}, \sigma_5 = \tau_{23}$, and $\sigma_6 = \tau_{12}$. Equation (51) is obviously very complicated thus it will restrict the above attention to the reduction of above equation for an orthotropic lamina under plane stress conditions:

$$\begin{aligned} &F_1\sigma_1 + F_2\sigma_2 + F_3\sigma_3 + F_{11}\sigma_1^2 + +F_{22}\sigma_2^2 + F_{33}\sigma_3^2 + F_{12}\sigma_1\sigma_2 \\ &+ F_{13}\sigma_1\sigma_3 + F_{23}\sigma_2\sigma_3 + F_{44}\sigma_4^2 + F_{55}\sigma_5^2 + F_{66}\sigma_6^2 = 1 \end{aligned} \qquad \textbf{(52)}$$

The terms that are linear in the stresses are useful in representing different strengths in tension and in compression. The terms that are quadratic in the stresses are the more or less usual terms to represent an ellipsoid in stress space, where $F_3 = 0$ indicates that to the shear strength of a material in compression and in tension is similar, and $\sigma_3 = 0$ in *z*-direction. Also, the shear strength of a material is equal in three dimensions and equal to ***S***. Thus, the terms of F_i is:

$$\begin{aligned} &F_1 = \left(\frac{1}{X_t} - \frac{1}{X_c}\right), F_2 = \left(\frac{1}{Y_t} - \frac{1}{Y_c}\right), F_3 = \left(\frac{1}{Z_t} - \frac{1}{Z_c}\right) \\ &F_{11} = \left(\frac{1}{X_t . X_c}\right), F_{22} = \left(\frac{1}{Y_t . Y_c}\right), F_{33} = \left(\frac{1}{Z_t . Z_c}\right) \\ &F_{44} = \left(\frac{1}{R^2}\right), F_{55} = \left(\frac{1}{S^2}\right), F_{66} = \left(\frac{1}{T^2}\right) \\ &F_{12} = \frac{-1}{2}\left(\frac{1}{X_t . X_c . Y_t Y_c}\right)^{0.5}, F_{13} = \frac{-1}{2}\left(\frac{1}{X_t . X_c . Z_c . Z_t}\right)^{0.5} \\ &F_{23} = \frac{-1}{2}\left(\frac{1}{Y_t . Y_c . Z_c . Z_t}\right)^{0.5} \end{aligned} \qquad \textbf{(53)}$$

where,

X_c, X_t = The axial or longitudinal strength in compression and tension.

Y_c, Y_t = The transverse strength in compression and tension.

Z_c, Z_t = The transverse strength in compression and tension.

R, T, S = Shear strength of the material.

Equation (52) becomes as:

$$F_1\sigma_1 + F_2\sigma_2 + F_{11}\sigma_1^2 + +F_{22}\sigma_2^2 + F_{12}\sigma_1\sigma_2 + F_{44}\sigma_4^2 + F_{55}\sigma_5^2 + F_{66}\sigma_6^2 = 1 \qquad (54)$$

Equation (54) is suitable for the elastic-plastic analysis of anisotropic materials.

For matrix cracking failure, two different failure criteria are used depending on whether the transverse normal stress, σ_{22}, is in tension or in compression. The failure index, e_m^2, is defined in terms of transverse tensile strength, Y_t , transverse compressive strength, Y_c, and in-plane shear strength, R, and is expressed as:

$$e_m^2 = \frac{\sigma_{22}}{Y_c}\left[\left(\frac{Y_c}{2R}\right)^2 - 1\right] + \left(\frac{\sigma_{22}}{2R}\right)^2 + \left(\frac{\tau_{12}}{R}\right)^2 \quad \text{for } \sigma_{22} < 0 \qquad (55)$$

and,

$$e_m^2 = \left(\frac{\sigma_{22}}{Y_t}\right)^2 + \left(\frac{\tau_{12}}{R}\right)^2 \quad \text{for } \sigma_{22} > 0 \qquad (56)$$

where (e_m) is the failure index for matrix cracking. Matrix cracking is assumed to occur when the failure index (e_m) exceeds unity.

Fiber-matrix shear failure is assumed to be dependent on a combination of axial stress, σ_{11}, and shear stress, τ_{12}, and is expressed as follows:

$$e_s^2 = \left(\frac{\sigma_{11}}{X_t}\right)^2 + \left(\frac{\tau_{12}}{R}\right)^2 \quad \text{for } \sigma_{11} > 0 \text{ and } \left(\frac{\sigma_{11}}{X_t}\right)^2 < \left(\frac{\tau_{12}}{R}\right)^2 \qquad (57)$$

and,

$$e_s^2 = \left(\frac{\sigma_{11}}{X_c}\right)^2 + \left(\frac{\tau_{12}}{R}\right)^2 \quad \text{for } \sigma_{11} < 0 \text{ and } \left(\frac{\sigma_{11}}{X_t}\right)^2 < \left(\frac{\tau_{12}}{R}\right)^2 \qquad (58)$$

where (e_s) is the failure index for fiber-matrix shearing, X_t is the tensile strength along the fiber direction and X_c is the compressive strength along the fiber direction. Equations (57) and (58) predict that when the failure (e_s) exceeds unity, fiber-matrix shearing dominated failure occurs.

Fiber breakage failure occurs in tension due to the combination of axial stress and shear stress while the failure in compression is governed by buckling as expressed in terms of only axial stress. The criterion for breakage failure is expressed as follows:

$$e_f^2 = \left(\frac{\sigma_{11}}{X_t}\right)^2 + \left(\frac{\tau_{12}}{R}\right)^2 \quad \text{for } \sigma_{11} > 0 \qquad (59)$$

and,

$$e_f^2 = \left(\frac{\sigma_{11}}{X_c}\right)^{2^2} \quad \text{for } \sigma_{11} < 0 \qquad (60)$$

where (e_s) is the failure index for fiber breakage. The fiber breakage failure occurs when (e_s) exceeds unity.

Applications and Discussions

In order to verify the reliability of the adopted numerical method, some case studies reported by other researchers are utilized. The study of the composite plate will be introduced.

Comparison with experimental investigation of composite plate

The post-buckling and failure characteristics of flat, rectangular graphite-epoxy panels with and without holes that are loaded in axial compression have been examined in an experimental study by **Starnes** and **Rouse** [**1981**] and in a theoretical study by **Elseifi** [**1998**][(7)]. The panels were fabricated from commercially available unidirectional Thornel 300 graphite-fiber tapes preimpregnated with 450 K cure Narmco 5208 thermosetting epoxy resin. Typical lamina properties for this graphite-epoxy system are 131.0 GPa for the longitudinal Young's modulus, 13.0 GPa for the transverse Young's modulus, 6.4 GPa for the in-plane shear modulus, 0.38 for the major Poisson's ratio ($\boldsymbol{v}_{12}$), and 0.14 mm for the lamina thickness. The loaded ends of the panel were clamped by fixtures during testing, and the unloaded edges were simply supported by knife-edge restrains to prevent the panels from buckling.

In the present study, the plate is analyzed by using nine-node isoparametric Lagrangian finite elements with nine degrees of freedom per node. The panel is 0.508 m long, 0.178 m wide, and 24-ply orthotropic laminate with $[(45^o/0^o/-45^o)_2, (45^o/0^o/-45^o)_2, (45^o/0^o/90^o)_4]$ stacking sequence. The modeling approach of the quarter plate was based on using two elements in the short direction, and three elements in the long direction. The finite element mesh used is shown in **Figure (7)**. In order to efficiently proceed beyond the critical buckling point in the post-buckling analysis of the panel, an initial geometric imperfection in the same shape as the first buckling mode was assumed. The amplitude of this initial imperfection is (1%) of the total laminate thickness. Figure (8) shows the out-of-plane deflection ($\boldsymbol{w}$) near a point of maximum deflection (node $\boldsymbol{i}$) normalized by the panel thickness $\boldsymbol{h}$ as a function of the normalized load. From this figure, it can be noticed that good agreement exists with the experimental results with a difference not more than (6%). On the other hand, the present results are closer to the experimental investigation.

Comparison with theoretical investigation of composite plate

A square cross-ply laminated plate with simply supported edges and initial imperfection was analyzed by **Zou** and **Qiao** [**2002**][(16)]. Lateral in-plane expansion is allowed at the loaded ends and the unloaded edges can be moved in the plane but remain straight. The layer material and geometry properties are presented in Figure (9). The slenderness ratio is set as ($\boldsymbol{b}/\boldsymbol{h}$=20), and it represents a moderately thick laminate. The laminated plate contains eight equal-thickness layers in $[0^o/90^o]_4$ layup. The initial imperfection ($\boldsymbol{w_o}/\boldsymbol{h}$) is given by (0.0 and 0.1) by which the shape is considered to be a sinusoidal curve. **Zou** and **Qiao** used higher order finite strip method and solved the nonlinear equations by **Newton-Raphson** method. In the present study, a quarter of the laminate is modeled with (2×2) mesh of nine-node isoparametric Lagrangian element with nine degrees of freedom per node. Numerical results and response comparisons with **Zou** and **Qiao** [**2002**][(16)] are shown in Figures (10) and (11) for axial load versus total deflection and axial load versus end shortening strain ($\boldsymbol{\varepsilon}$). The present results are really close to those of **Zou** and **Qiao** [**2002**][(16)] with a difference of not more than (15%).

Parametric Study

A parametric study is performed to assess the influence of several important parameters on the elastic-plastic large displacement analysis of a composite laminated plate subjected to in-plane compressive load.

The selected parametric studies are summarized as follows:

1. The effect of through-thickness shear deformation.
2. The effect of fiber's orientation angle.
3. The effect of degree of orthotropy of individual layers.
4. The effect of fiber waviness.

Each one of the above parameters was studied individually by analyzing a type of laminated composite plate. In all cases, a nine-node element was used and also one quadrant of the plate was analyzed due to symmetry and (2×2) mesh is used in the cross-ply and straight fiber plates while for angle-ply and sine wave fiber plates, were analyzed by considering the full plates with (4×4) element mesh. Lateral in-plane expansion is allowed at the loaded ends and the unloaded edges can be moved in the in-plane direction but remain straight. The initial imperfection shape is considered to be a sinusoidal curve. The following geometry and layer material properties of high graphite epoxy are used in the analysis: (E_1=172.5 GPa; E_2=7.08 GPa; G_{12}=G_{13}=3.45 GPa, G_{23}=1.38 GPa; E_f=341.42 GPa; E_m=3.58 GPa; V_f=0.5; V_m=0.5; ν_{12}=ν_{13}=ν_{23}=0.25, X_t=X_c=1450 MPa, Y_t=36 MPa, Y_c=230 MPa, S=62 MPa)[**Parhi**, **et al.**, **2001**][83]. The geometry properties are (a=1.0 m, a/b=1).

1. Effect of through-thickness shear deformation

To show the effect of transverse shear deformation on the large displacement elastic-plastic analysis of laminated composite plate under in-plane compressive load, a simply supported plate with a range of slenderness ratio (b/h) from (20) to (120), with symmetric cross-ply and antisymmetric cross-ply arrangement and with six layers was analyzed. The initial imperfection is (w_o/h= 0.1) by which the shape is considered to be a sinusoidal curve.

Figures (12) and (13) present the load-deflection curves of the symmetric cross-ply, and the antisymmetric cross-ply laminated composite plate under in-plane loading and with slenderness ratio (b/h=20) by taking the effects of transverse shear deformation through the degrees of freedom per node of the element.

Figures (14) and (15) show the effect of shear deformation of symmetric cross-ply, and antisymmetric cross-ply laminated composite plate under in-plane loading with range of slenderness ratio(b/h) (20-120).

2. Effect of fiber's orientation angle

To study the effect of fiber's orientation angle on the large displacement elastic-plastic analysis of laminated composite plates under in-plane compressive load, a square simply supported laminated plate with two layers was analyzed. The initial imperfection is neglected in the present study.

Figure (16) shows the effect of fiber's orientation on the nonlinear analysis of composite laminated plate under in-plane compressive load. From this figure, it could be noticed that the ultimate strength of the plate with ($0^o/90^o$) gives ultimate load (651.2 kN/m). This orientation's fiber means that it is the optimum for a plate under in-plane compressive load.

3. Effects of fiber waviness

To show the effect of fiber waviness on the large displacement elastic-plastic analysis of laminated composite plate, a square simply supported plate, with six layers was considered. The shape of fiber was considered to follow a sinusoidal curve. The effects of this type are (number of sequence (k), amplitude of wave (Δ), and fiber's orientation. The initial imperfection (w_o/h= 0.1) by which the shape is considered to be sinusoidal curve. The value of amplitude of sine wave fiber is varying (Δ=0.05-0.5) and the number of sequences of the sine wave fiber (k) was considered changeable in the range of (1-12).

Figures (17) and (18) present the load-deflection curves of laminated with symmetric cross-ply composite plate under in-plane compressive load and with sine wave fibers with a range of amplitude (0.05-0.5).

Figures (19)-(22) present the ultimate strength-fiber path amplitude (Δ) curves for the laminated, with symmetric cross-ply, and antisymmetric cross-ply composite plates under in-plane compressive load and with a range of number of sequences (k) (1-12), respectively.

Conclusions

A nonlinear finite element method is adopted for the large displacement elastic-plastic static analysis of anisotropic plates under in-plane compressive load. Many of effects were considered in the present study such as the effect of orthotropy of individual layers, through-thickness shear deformation, fiber's orientation angle, and fiber waviness on the large displacement elastic-plastic static analysis. The following conclusions are drawn with regard to the results obtained for the anisotropic plates under in-plane static loading as follows, 1) The capacity of a laminated plate with sine wave fiber under in-plane compressive load in the direction of waviness is more than the capacity of the plate under in-plane compressive load orthogonal to the direction of waviness by (42%) for a plate with sine wave fiber (k=12, Δ=0.4). 2) The ultimate strength of a cross-ply laminated plate is greater than the ultimate strength of an angle-ply laminated plate with the same laminas. 3) The ultimate strength of a symmetric cross-ply laminated plate is greater than the ultimate strength of an antisymmetric cross-ply laminated plate with the same laminas. 4) A symmetric cross-ply laminated plate with sine wave fiber (k=12, Δ=0.4) gives in-plane loading (610 kN/m) and this represents the peak capacity and this case is the best.

References

1. Abid-Ali, A. K., "Stress Analysis of Laminated Fiber Reinforced Composite Cylinder", M.Sc. Thesis, University of Babylon, Hilla, Iraq, 2000.
2. Ali, N. H., "Finite Element Dynamic Analysis of Laminated Composite Plates Including Damping Effect", M.Sc. Thesis, University of Babylon, Hilla, Iraq, 2004.
3. Amash, H. K., "Post-buckling and Post-Yielding Analysis of Imperfect Thin Plate by Finite Difference Method", M.Sc. Thesis, University of Babylon, Hilla, Iraq, 2003.
4. Amash, H. K., "Nonlinear Static and Dynamic Analysis of Laminated Plates Under In-plane Forces", Ph.D. Thesis, University of Babylon, Hilla, Iraq, 2008.
5. Chia, C.Y., "Nonlinear Analysis of Plates", McGraw-Hill International Book Company, 1980.
6. Cook, R.D., "Finite Element Modeling for Stress Analysis", John Wiley & Sons, Inc., 1995.
7. Elseifi, M., "A New Scheme for the Optimum Design of Stiffened Composite Panels with Geometric Imperfections", Ph.D. Thesis, Virginia Polytechnic Institute, U.S.A., 1998.
8. Hashin, Z. "Failure Criteria for Unidirectional Fiber Composites", ASME, J. Appl. Mech., Vol.47, 1980, pp.329-334.
9. Jones, R.M., "Mechanics of Composite Materials", Second Edition, Taylor and Francis Inc., U.S.A., 1999.
10. Kaw, A., "Mechanics of Composite Materials", Second Edition, Taylor and Francis Group, LLC, 2006.
11. Kommineni, J. R., and Kant, T. "Geometrically Non-linear Transient C^o Finite Element Analysis of Composite and Sandwich Plates with a Refined Theory." Struct. Eng. And Mech., Vol.1, No.1, 1993, pp87-102.
12. Pandey, M. D., "Effect of Fiber Waviness on Buckling Strength of Composite Plates." ASCE, J. Eng. Mech., Vol.125, No.10, 1999, pp.1173-1179.
13. Pica, A., Wood, R.D., and Hinton, E. "Finite Element Analysis of Geometrically Nonlinear Plate Behavior Using a Mindlin Formulation." Comp. & Struct., Vol.11, 1979, pp.203-215.
14. Pica, A., Wood, R.D "Post-Buckling Behavior of Plates and Shells Using a Mindlin Shallow Shell Formulation." Comp. & Struct., Vol.12, 1980, pp.759-768.
15. Shukla, K.K., and Nath, Y., "Thermomechanical Post-Buckling of Cross-Ply Laminated Rectangular Plates", ASCE, J. Eng. Mech., Vol.128, No.1, 2002, pp.93-101.
16. Zou, G., and Qiao, P., "Higher Order Finite Strip Method for Post-Buckling Analysis of Imperfect Composite Plates" J. Eng. Mech., Vol.128, No.9, Sep., 2002, pp.1008-1015.

Table (1): Comparison of results with experimental and theoretical studies of composite laminated plate under in-plane compressive load in x-direction, (a/b=2.854, w_o/h=0.1)

Load (P_x/P_{cr})	Max. Deflection ($(w+w_o)/h$)		
	Experimental results(*)	Theoretical results[31]	Present study
0.00	0.010	0.010	0.010
0.10	0.021	0.020	0.013
0.30	0.042	0.030	0.017
0.60	0.063	0.060	0.035
0.75	0.125	0.110	0.064
0.90	0.310	0.280	0.210
1.10	0.850	0.645	0.770
1.28	1.176	1.021	1.122
1.50	1.580	1.380	1.495
1.60	1.720	1.500	1.645
1.80	2.020	1.720	1.930
1.90	2.166	1.810	2.068
2.00	2.333	1.900	2.203

* : Given by **Starnes** and **Rouse** [**1981**] as mentioned in **Elseifi** [**1998**][7].

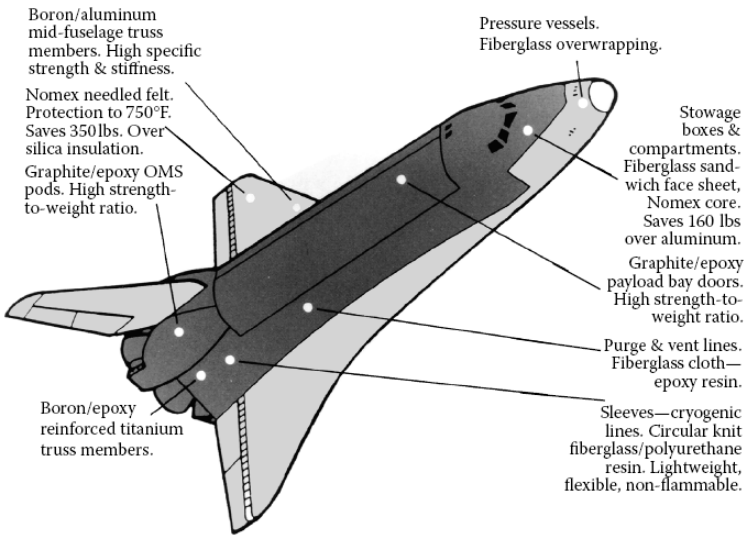

Figure (1): Use of composites in the space shuttle [**Kaw,2006**][10]

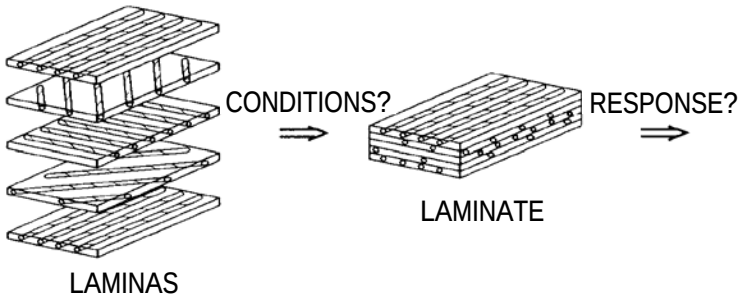

Figure (2): Laminated plate with several lamina orientations[**Jones, 1999**](9)

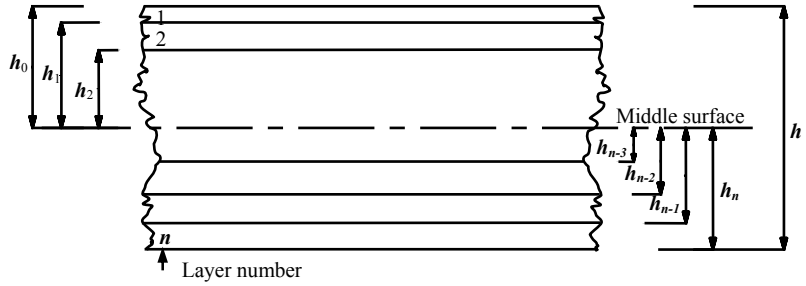

Figure (3): Geometry of an NL-layered laminate [**Jones,1999**](9)

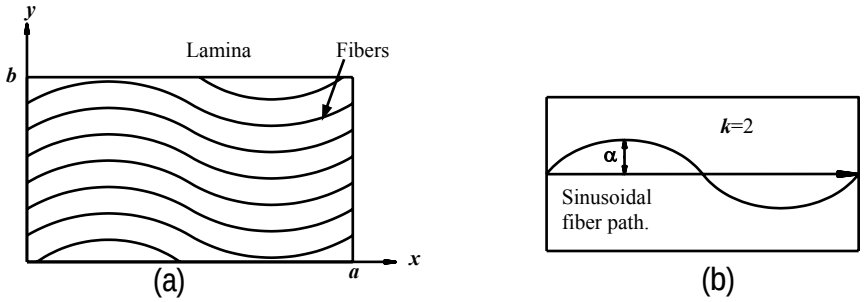

Fiber (4): (a) Lamina with variable fiber orientation; (b) Geometry of sinusoidal fiber path [**Pandey,1999**](12)

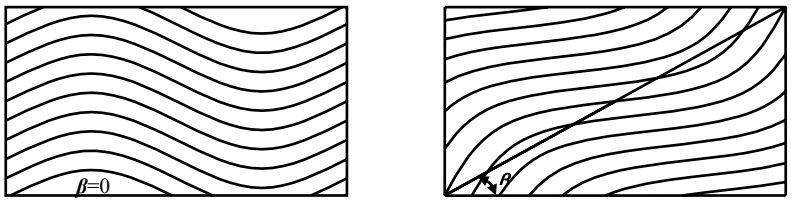

Figure (5): Laminate plate with sine wave fibers aligned with ***x***-axis

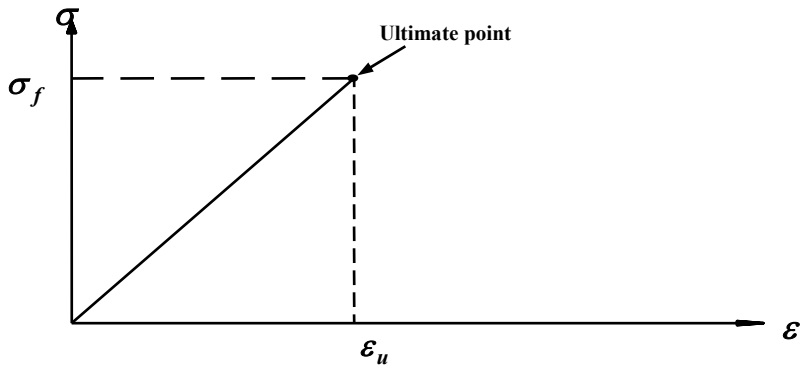

Figure (6): Idealizated stress-strain relationship of uniaxial loading behavior for orthrotropic plate[**Jones, 1999**](9)

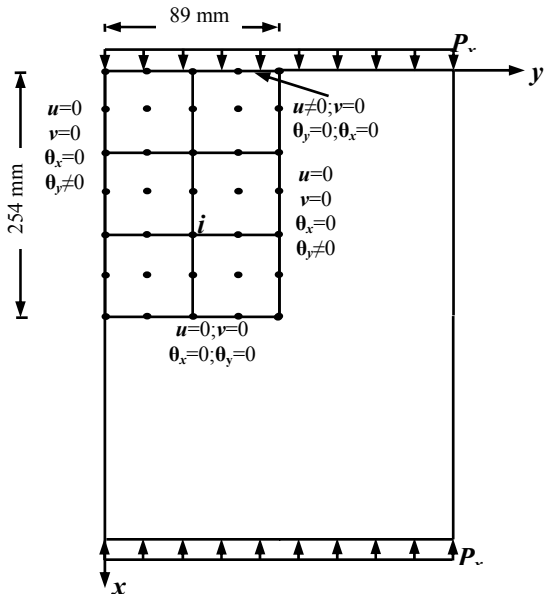

Figure (7): Finite element mesh and boundary condition for the quarter of the composite plate under in-plane compressive load ir x-direction

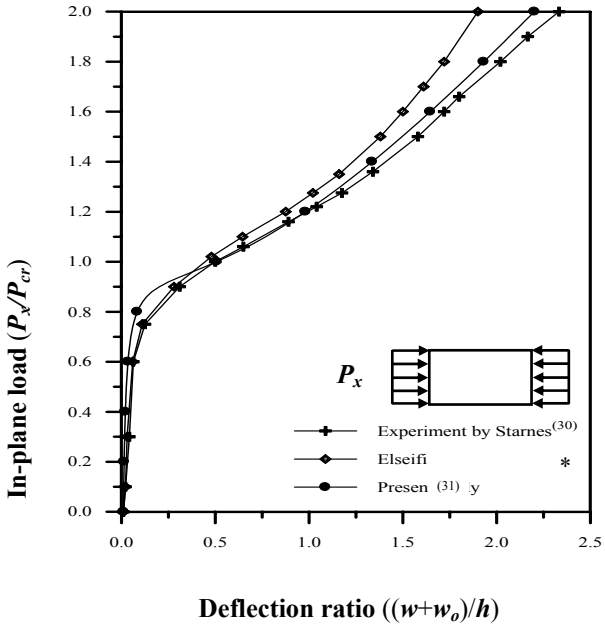

Figure (8): Post-buckling curve for a rectangular thin composite laminated plate under in-plane compressive load in x-direction

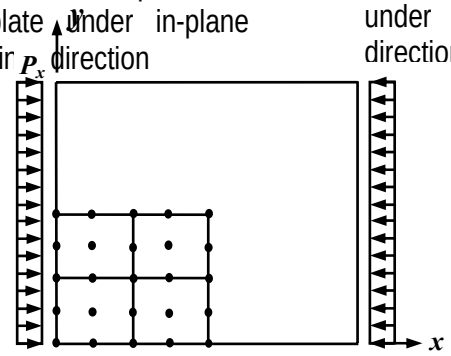

a=200 (mm)
b=200 (mm)
h=10 mm
E_1/E_2=20
$G_{12}/E_2=G_{13}/E_2$=0.6
G_{23}/E_2=0.5
E_2=10 GPa
$\nu_{12}=\nu_{13}=\nu_{23}$=0.25

Figure (9): Details of a square laminated composite plate under in-plane compressive load and material properties

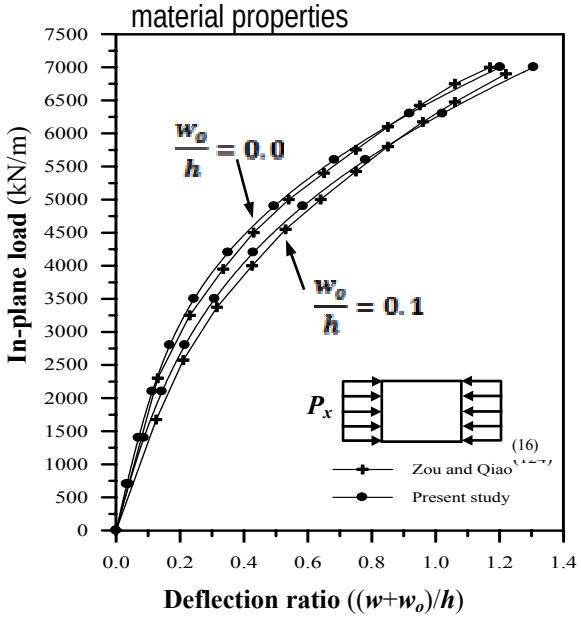

Figure (10): Load-deflection curve of antisymmetric cross-ply imperfect rectangular thick composite laminated plate under compressive load,(b/h=20, a/b=1)

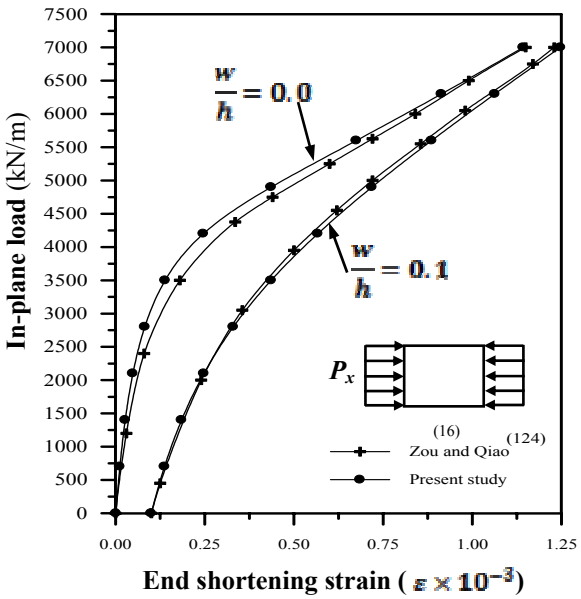

Figure (11): Load-end shortening strain curve of antisymmetric cross-ply imperfect rectangular thick composite laminated plate under compressive load,(b/h=20, a/b=1)

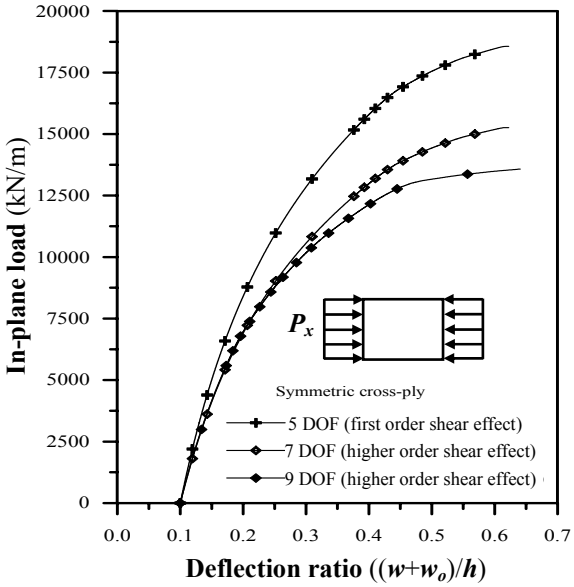

Figure (12): Load-deflection curve of symmetric cross-ply imperfect square composite laminated plate under in-plane compressive load with (b/h=20;a/b=1;w_o/h=0.1)

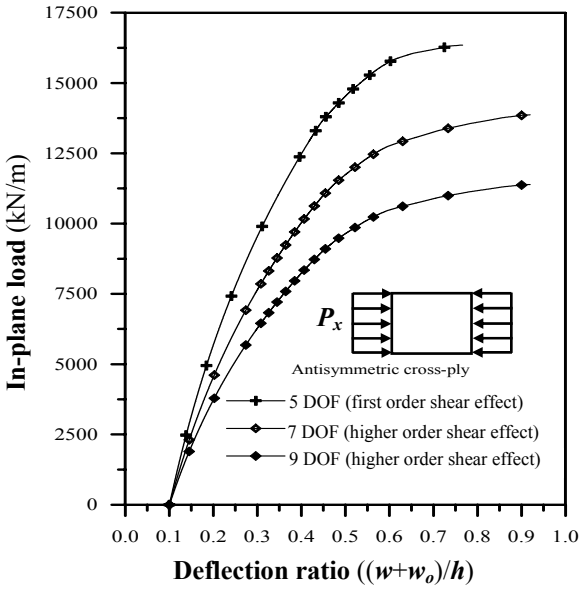

Figure (13): Load-deflection curve of antisymmetric cross-ply imperfect square composite laminated plate under in-plane compressive load with (b/h=20;a/b=1; w_o/h=0.1)

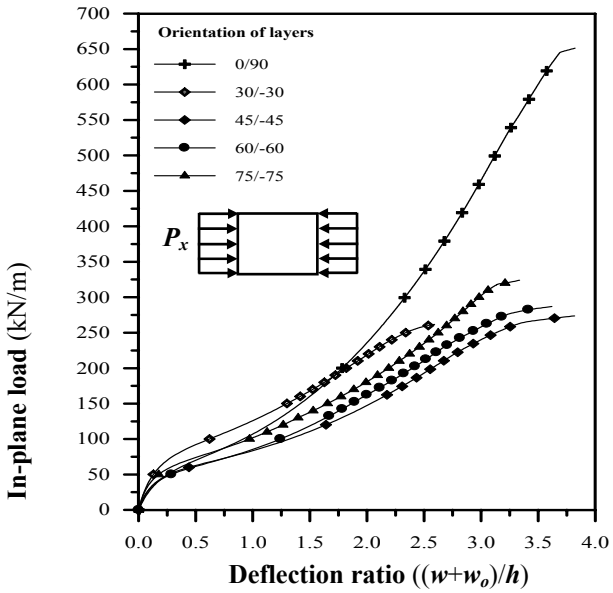

Figure (16): Effect of orientation's fiber on the large displacement elastic-plastic analysis of composite laminated plate under in-plane compressive load (b/h=100; w_o/h=0.0;a/b=1)

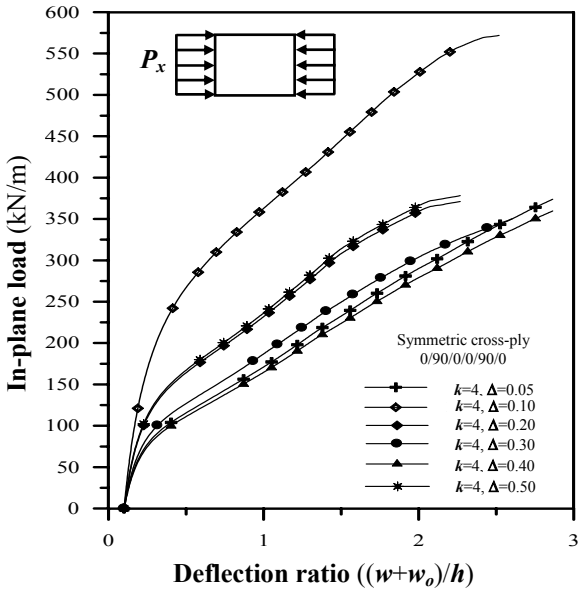

Figure (17): Load-deflection curve of simply supported square laminated composite plate with sine wave fiber with a range of fiber amplitude (0.05-0.50) and under in-plane compressive load, (w_o/h =0.1;b/h=100;a/b=1.0;k=4)

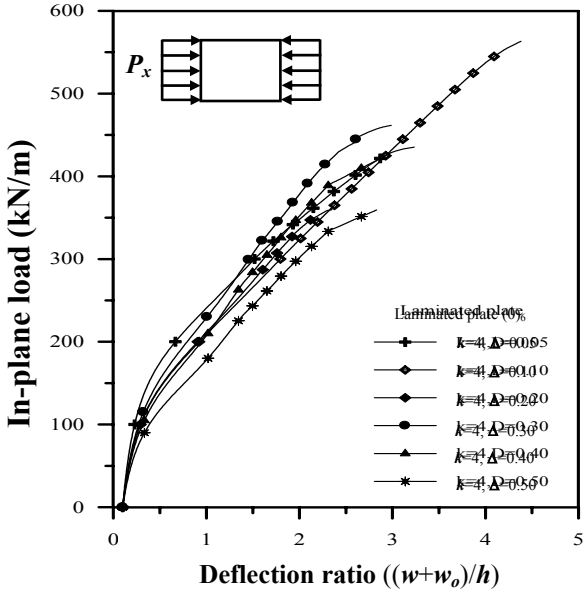

Figure (18): Load-deflection curve of simply supported square symmetric cross-ply composite plate with sine wave fiber with a range of fiber amplitude (0.05-0.50) and under in-plane compressive load, (w_o/h =0.1;b/h=100;a/b=1.0;k=4)

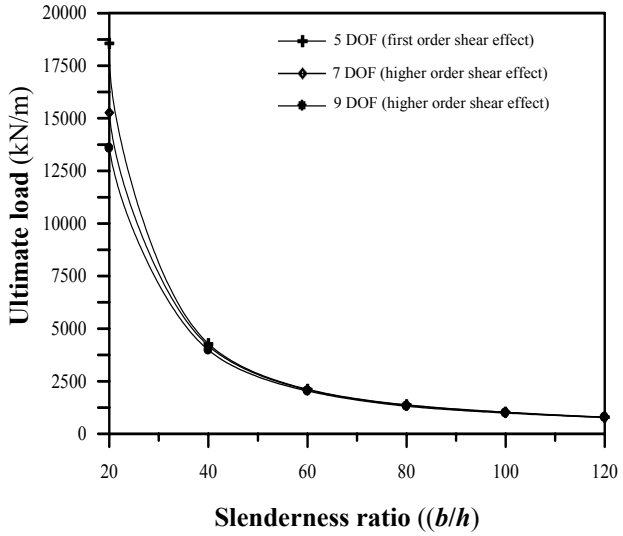

Figure (14): Effect of number of degrees of freedom on the large elastic-plastic analysis of symmetric cross-ply composite laminated plate under in-plane compressive load with a range of slenderness ratio (b/h)

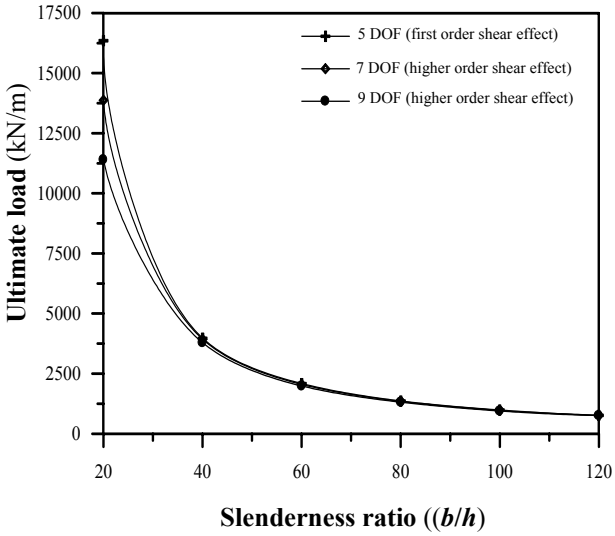

Figure (15): Effect of number of degrees of freedom on the large elastic-plastic analysis of antisymmetric cross-ply composite laminated plate under in-plane compressive load with a range of slenderness ratio (b/h)

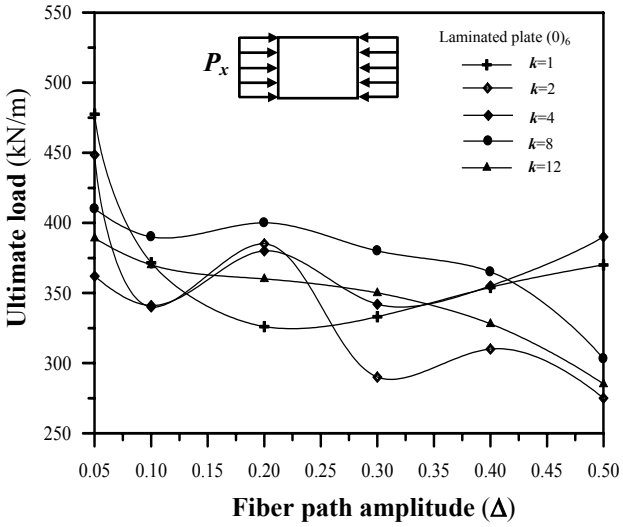

Figure (19): Ultimate load-fiber path amplitude curve of simply supported square laminated composite plate under in-plane compressive load in *x*-direction and with a range of number of sequences (1-12),(w_o/h= 0.1, b/h=100, a/b=1.0)

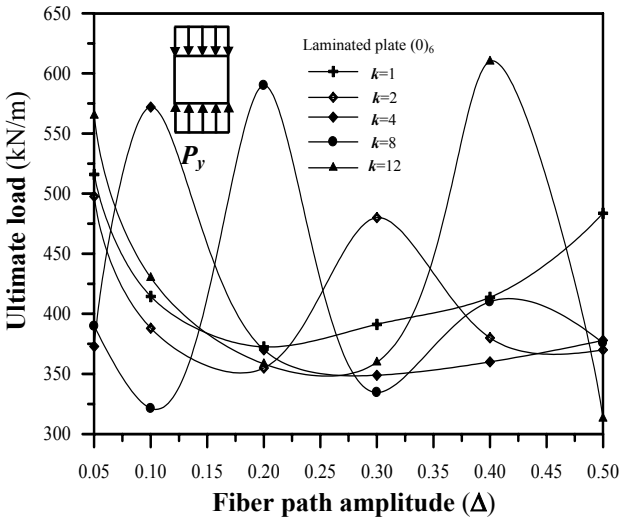

Figure (20): Ultimate load-fiber path amplitude curve of simply supported square laminated composite plate under in-plane compressive load in *y*-direction and with a range of number of sequences (1-12),(w_o/h=0.1, b/h=100, a/b=1.0)

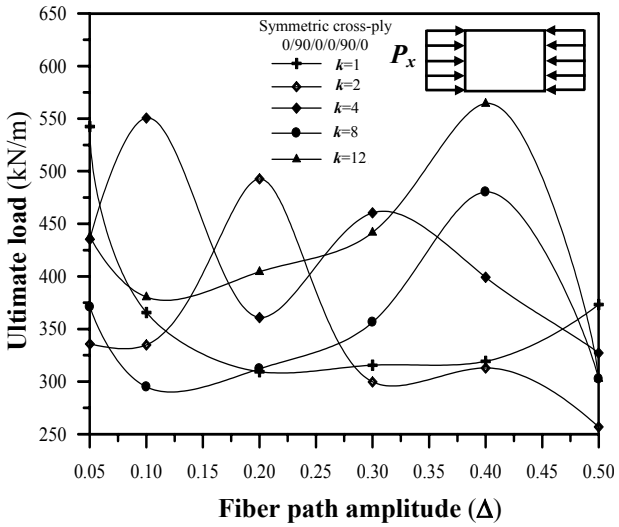

Figure (21): Ultimate load-fiber path amplitude curve of simply supported square symmetric cross-ply composite plate under in-plane compressive load and with a range of number of sequences (1-12),(w_o/h= 0.1, b/h=100, a/b=1.0)

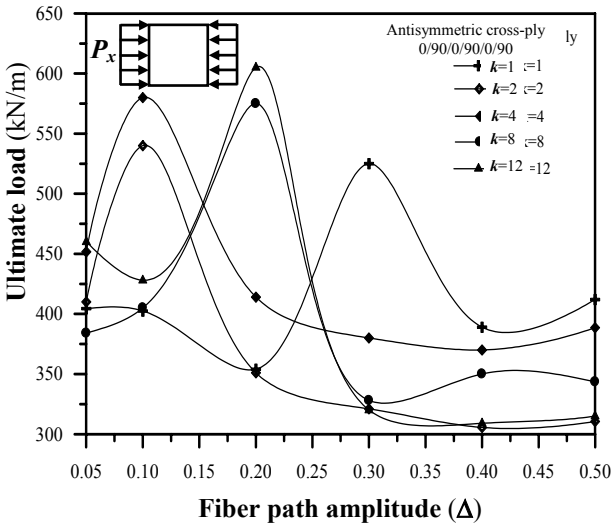

Figure (22): Ultimate load-fiber path amplitude curve of simply supported square antisymmetric cross-ply composite plate under in-plane compressive load and with a range of number of sequences (1-12),(w_o/h= 0.1, b/h=100, a/b=1.0)